Proceedings of the Twenty-second (2012) International Offshore and Polar Engineering Conference
Rhodes, Greece, June 17–22, 2012

ISBN 978-1-880653-94–4 (Set); ISSN 1098-6189 (Set)

www.isope.org

Investigation of Wave Transmission from a Floating Wave Dragon Wave Energy Converter

Jørgen Harck Nørgaard and Thomas Lykke Andersen
Aalborg University, Department of Civil Engineering
Aalborg, Denmark

ABSTRACT

This paper focuses on the calibration of the MIKE21BW model against the measured wave height reduction behind a 24 *kW/m* Wave Dragon (WD) wave energy converter. A numerical model is used to determine the wave transmission through the floating WD in varying wave conditions. The transmission obtained from the MIKE21BW model is compared to results from a simpler model, based on the integration of wave energy flux. The conclusion is that the simplified approach provides results similar to the transmission obtained from the numerical model, both for a single WD and a farm of multiple WDs.

KEY WORDS: Wave energy converter, wave transmission, physical tests, numerical modelling, coastal protection

INTRODUCTION

Floating Wave Energy Converters (WECs) can be positioned offshore to harvest energy from waves. Since the energy is conserved the incident wave energy is absorbed, transmitted, and reflected by the WEC device and consequently the wave height behind the device is reduced. Especially in the context of increasing water levels caused by climate changes, the wave height reduction can provide mitigation of flooding and coastal erosion hazards. This additional benefit can help introduce WECs as a green alternative to other types of structures used for coastal protection.

A significant amount of research has been carried out on hydrodynamic behaviour of oscillating WECs. Several researchers have concentrated on the performance of wave energy devices positioned in arrays in order to optimize electricity production. However, recent studies such as (Venugopal and Smith, 2007), (Palha et al., 2010), (Beels et al., 2010a), and (Ruol et al., 2011) have also focused on the wake of a single WEC or multiple WECs in order to optimize the wave height reduction behind the devices and to evaluate the impact of the wake effects on the shoreline. Numerical wave propagation models have proven to be powerful tools in such studies, since these can be used to analyse the effect of a WEC farm on a specific bathymetry.

Venugopal and Smith (2007) evaluated the change in wave climate behind an array of hypothetical WECs with hypothetical transmission characteristics offshore of the Orkney Islands. They used the depth integrated MIKE21BW Boussinesq model where partial reflecting and partial transmitting WECs were implemented as porous structures with changing transmission/reflection properties depending on the wave conditions.

In the study by Palha et al. (2010), the depth integrated, mild-slope REFDIF model was adapted to study the impact of wave energy absorption by a farm of Pelamis WECs at the near-shore wave climate on the west coast of Portugal. Three different sinusoidal incident wave conditions were considered, and five different WEC farm configurations were analysed. The wave transmission from the WECs was specified from the energy absorption estimated by the developer.

Beels et al. (2010a) performed a detailed study of the Wave Dragon device (WD) implemented in the depth integrated, mild-slope numerical wave propagation model MILDwave. The MILDwave model was calibrated against the transmitted wave power obtained by analytical integration of energy from the draft of the device to the seabed, as described in Beels et al. (2010b). The wave height reduction behind a single WD and multiple WDs respectively was studied in detail for long crested and short crested waves.

Ruol et al. (2011) evaluated the hypothetical application of the DEXA wave energy converter for coastal protection in a case study at an Italian site, Marina di Ravenna beach. Based on the simplified CERC formula, long-shore sediment transport was evaluated in the presence and absence of a single line of equally spaced DEXA devices. The wave energy transmission from the DEXA device was based on the physical tests by Zanuttigh et al. (2010), performed in the deep water wave basin at Aalborg University, Denmark. Ruol et al. (2011) concluded that a DEXA farm only had a modest effect on wave attenuation, and a more evident effect on net sediment transport.

MOTIVATION FOR THE PRESENT STUDY

The aforementioned studies by Venugopal and Smith (2007), Palha et al. (2010), and Beels et al. (2010a) respectively, using numerical wave propagation models, have not been validated against the actual measured wave height reduction behind the devices. Moreover, they used depth integrated models to evaluate the wake from floating devices and thus the effect of the heave/surge/pitch- movements of the devices was neglected. Detailed information on absorption and reflection is needed to accurately determine the wave transmission from a single or multiple devices in various sea conditions. This requires scaled, physical model tests in a laboratory basin, where the wave disturbance close to a single device is measured.

Ruol et al. (2011) evaluated a line of several DEXAs with individual wave transmission characteristics obtained from the wave transmission measured from physical tests of a single device. The wave transmission from a single device was assumed to be unaffected by the presence of side-lying devices. Physical tests or simulations in a calibrated wave propagation model on side-lying devices are needed to validate this assumption.

In the present paper, the data from the model test study by Nørgaard et al. (2011) is considered. The tests were conducted in a shallow wave basin at Aalborg University in a 1:51.8 scale of the 24 *kW/m* WD. Wave disturbance measurements from the model tests are used for calibration of the depth integrated, numerical MIKE21BW Boussinesq wave propagation model. The calibrated model is used to determine the wave height reduction in a distance far from the devices. Moreover, the model is used for determining the overall wave transmission from a single WD and multiple WDs in different wave climates without the influence from model boundaries. Different mooring stiffness are evaluated as in the physical model in order to study the influence of heave/surge/pitch movements on wave transmission from the device. Results are compared to the transmission coefficients obtained by wave power integration.

CONSIDERED DEVICE

The WD consists of two main elements reflectors and a main body. The reflectors focus the incoming waves towards a doubly curved ramp on the main body where the waves overtop into a water reservoir above mean sea level. Dimensions of the considered prototype scale 24 *kW/m* WD are given in Fig. 1.

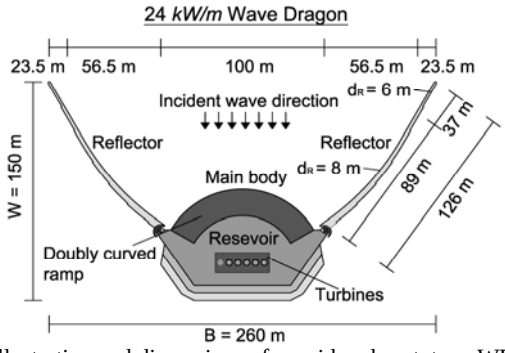

Fig. 1. Illustration and dimensions of considered prototype WD model.

Electricity is produced from a set of low head, hydro turbines when the water in the reservoir drains through the turbines. The WD is moored and able to turn and face the mean incident wave direction. An advanced pneumatic system is used to adjust the floating level of the WD and thereby adjust the overtopping rate. This is done in order to maximize the energy captured for a given wave climate.

As illustrated in Fig. 1, each reflector has a draft of 8 *m* at the WD shoulder over a length of 89 *m*, followed by a 37 *m* long section with decreasing draft to 6 *m* at the reflector tip. The varying draft along the reflectors is expected to provide varying transmission along the reflector length. The draft along the main body is constant. A definition sketch of the reflection/transmission/absorption from the WD reflectors and body is given in Figure 2. Subscripts in Figure 2 are: Wave power *p*, reflector *R*, main body *B*, incident *i*, transmission *t*, reflection *R*, and absorption *a*.

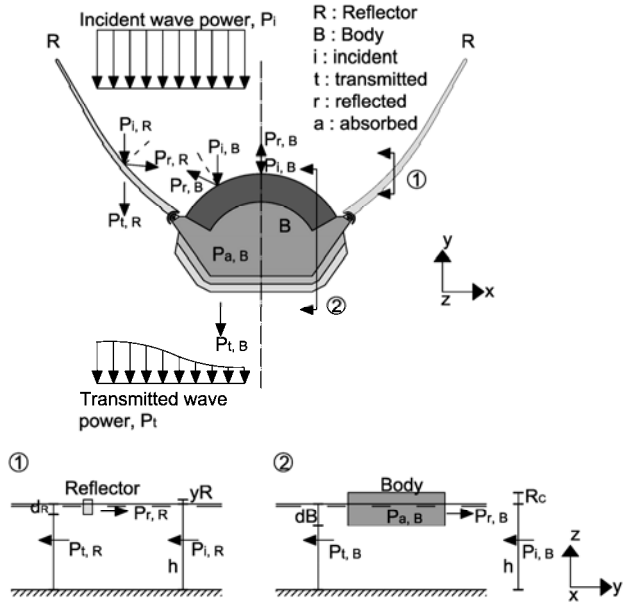

Fig. 2. Definition sketch and illustration of the reflection and transmission from the WD.

SIMPLE TRANSMISSION MODEL

The simplified model for determining the wave transmission through the WD is based on wave power integration below the draft of the floating structure. All wave power from the draft to the seabed is thus assumed to be fully transmitted. The simplified approach neglects the possible wave radiation generated from the floating device due to heave/surge/pitch movement.

The WD reflectors and WD body are evaluated separately due to different transmissive behaviour of the two components. The approach is described in the following starting with the wave transmission from the WD reflectors.

Reflectors

Kramer and Frigaard (2002) concluded with a BEM model the efficiency of the WD reflectors by considering the increase in wave power between the reflector shoulders compared to the incident wave power in the undisturbed area. The model was validated against laboratory tests with typical Danish wave situations in the North Sea. The study resulted in the efficiency factors, η_{eff}, in Table 1 for the increase in wave power in different wave situations. η_{eff} is calculated as the ratio between the mean wave power in the cross-section and the

wave power of the undisturbed incident wave. In Table 1, H_s is the significant wave height and T_p is the peak wave period.

Table 1. Efficiency of WD reflectors determined by Kramer and Frigaard (2002) in various wave conditions.

H_s [m]	1	2	3	4	5
T_p [s]	5.6	7.0	8.4	9.8	11.2
Efficiency, η_{eff}	1.86	1.45	1.24	1.20	1.15

The range of wave periods considered in (Kramer and Frigaard, 2002) is expanded to include T_p = 14 s in Figure 3, by extrapolating the efficiencies from Table 1. The expanded range will be used later when comparing against physical test results from Nørgaard et al. (2011).

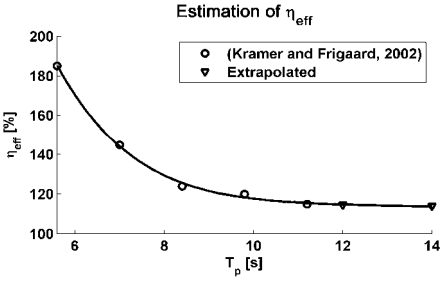

Fig. 3. Extrapolated efficiencies of wave reflectors from Table 1.

The ratio between the time of averaged reflected wave power (over one period) above the draft and the incident wave power at a given position with a specific draft d and depth h, is given in Eq. 1, based on linear wave theory (Kofoed and Burcharth, 2002). It is assumed that all energy above the draft is reflected (i.e. no overtopping of the reflector).

$$\lambda(f,d) = \frac{p_r(f,d)}{p_i(f)} \Downarrow$$
$$\lambda(f,d) = 1 - \frac{\sinh\left(2\cdot k(f)\cdot h\left(1-\frac{d}{h}\right)\right) + 2\cdot k(f)\cdot h\left(1-\frac{d}{h}\right)}{\sinh\left(2\cdot k(f)\cdot h\right) + 2\cdot k(f)\cdot h} \quad (1)$$

Conservation yields:

$$p_i = p_a + p_r + p_t \quad (2)$$

p_a [W/m] is the absorbed wave power, p_t [W/m] is the transmitted wave power, p_r [W/m] is the reflected wave power, and p_i [W/m] is the incident wave power.

Assuming that no wave absorption from the reflectors is present, the transmitted wave power under the reflectors, $p_{t,R}$, can be written as:

$$\begin{aligned} p_{t,R}(f,d_R) &= p_{i,R}(f) - p_{r,R}(f,d_R) \\ &= p_{i,R}(f)\cdot\left(1-\frac{p_{r,R}(f,d_R)}{p_{i,R}(f)}\right) \\ &= p_{i,R}(f)\cdot\left(1-\lambda(f,d_R)\right) \end{aligned} \quad (3)$$

The rate of transmitted wave power $p_{t,R}/p_{i,R}$ under the reflectors is determined for all frequencies in the JONSWAP spectrum for varying WD sizes - to peak period wave length, W/L_p (see definition of W and B in Fig. 1), and for h = 25 m. Results are plotted in Fig. 4

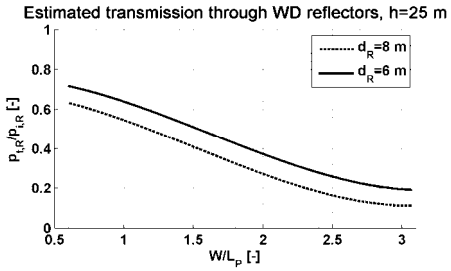

Fig. 4. Estimated rate of transmitted wave power through WD reflectors.

Main Body

The WD body converts wave energy into electricity from overtopped waves. Thus, a part of the incident wave power is absorbed, $p_{a,b}$, and reflected, $p_{r,b}$, on the WD body. The actual value of the absorbed and reflected wave power on the ramp is unimportant in the present work, since only the transmitted wave power, $p_{t,B}$, is of interest. When considering the wave transmission from the WD, all wave power below the draft, d_B, is again assumed to be fully transmitted under the main body. Thus, the transmitted wave power can be determined using the expression in Eq. 4.

$$\begin{aligned} p_{t,B}(f,d_B) &= p_{i,B}(f)\cdot\eta_{eff}(T_p) - \left(p_{r,B}(f,d_B) + p_{a,B}(f,d_B)\right) \\ &= p_{i,B}(f)\cdot\eta_{eff}(T_p)\cdot\left(1-\lambda(f,d_B)\right) \end{aligned} \quad (4)$$

The sensitivity of the relative floating ratio, R_c/H_s, to the production efficiency of the WD was investigated in Frigaard et al. (2006). In the study, the maximum efficiency was reached for a relative floating ratio of R_c/H_s = 0.8 to 1.

By using a relative floating level of R_c/H_s = 0.9 and a water depth of h = 25 m, the ratio of transmitted wave power is plotted in Fig. 5 for varying W/L_p. The ratio is determined for all frequencies in the JONSWAP spectrum. It should be noted that the extrapolated efficiency of the reflectors η_{eff} for wave periods outside the range investigated by Kramer and Frigaard (2002) is used for the determination of $p_{t,B}/p_{i,B}$.

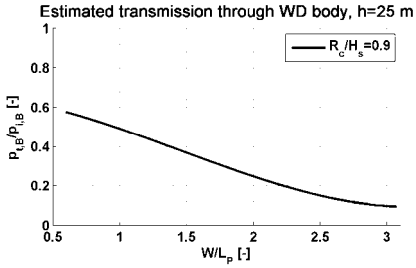

Fig. 5. Estimated rate of transmitted wave power through WD body.

Overall Transmission Coefficient from a Single WD

The overall wave transmission coefficient, $K_{t,tot}$, is calculated based on different sections for the body and the reflectors. According to the dimensions presented in Fig. 1, the total transmission coefficient can be obtained using the expression in Eq. 5.

$$K_{t,tot} = \sqrt{\frac{p_{t,R,dr=6}\cdot 23.5m\cdot 2 + p_{t,R,dr=8}\cdot 56.5m\cdot 2 + p_{t,B}\cdot 100m}{p_i\cdot 260m}} \quad (5)$$

$K_{t,tot}$ is plotted for varying W/L_p in Fig. 6. Again, the wave transmission is determined for all frequencies in the JONSWAP spectrum. As seen, the wave transmission coefficient increases for increasing wave length, meaning that a higher wave height reduction is present for smaller peak wave lengths - as expected.

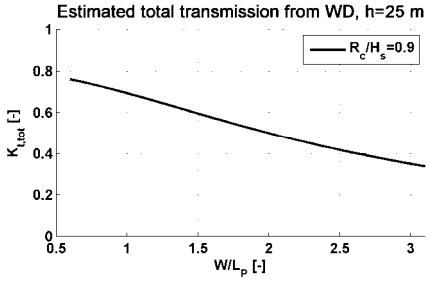

Fig. 6. Estimated rate of transmitted wave power through WD reflectors/body, and estimated overall transmission coefficient from WD.

PHYSICAL MODEL TEST SETUP

The test setup and test results from the physical tests on the measured wave height reduction behind the WD are described in detail in Nørgaard et al. (2011). The wave disturbance coefficient, $K_d = H_{s,measured}/H_{s,i}$, in the area close to the 260 *x* 150 *m* 24 *kW/m* WD, was measured in a 1:51.8 scale in a total of 90 tests. A photo from the laboratory tests at Aalborg University is presented in Fig. 7. The geometry and mass distribution of the laboratory WD model was based on the 1:4.5 Wave Dragon prototype designed for Nissum Bredning, Denmark, further described in Hald and Frigaard (2001).

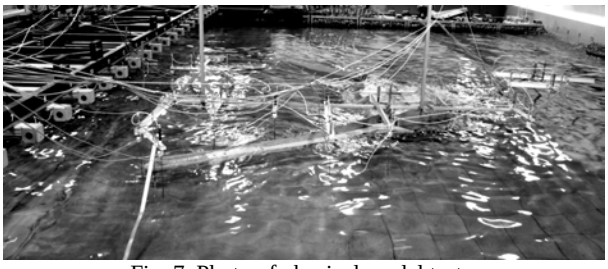

Fig. 7. Photo of physical model tests.

The wave gauge positions in the laboratory basin and the arrangement of the mooring system is illustrated in Fig. 8.

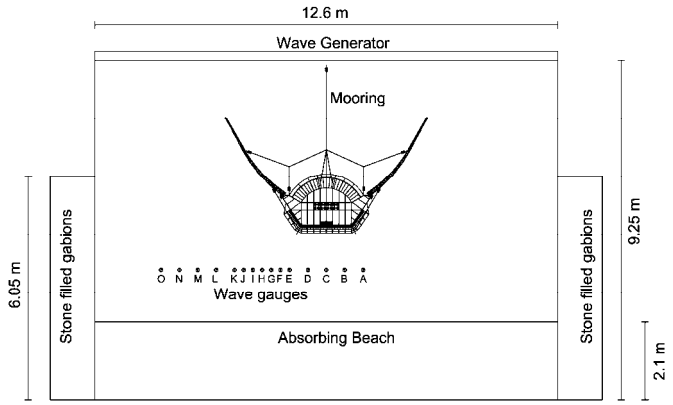

Fig. 8. Wave gauge positions.

The tests evaluated the influence of incident wave conditions together with mooring stiffness and floating ratios on the wave transmission/absorption characteristics. Irregular long-crested waves based on JONSWAP wave spectrum with $\gamma = 3.3$ were used in the model tests. Two different mooring setups were considered. In the *"normal"* mooring setup, the heave/surge/pitch movements of the WD were controlled by applying springs in the moorings with pre-stress as recommended in Hald and Frigaard (2001). In the *"fixed"* mooring setup, the WD was fixed in all its degree of freedom using vertically adjustable supports, which were fixed to the floor. The *"fixed"* mooring setup is not possible practically in the prototype scale, but is used as a reference to evaluate the influence from the movements of the WD on the wave transmission.

PHYSICAL MODEL TEST RESULTS

From the tests by Nørgaard et al. (2011), it was concluded that the wave transmission from the WD was more sensitive to the wave steepness, H_s/L_p, than the floating ratio. Moreover, the mooring stiffness had a significant influence on the wave height reduction behind the WD.

The variation of K_d, measured in a line behind the WD from the centre of the main body to the reflector tip, is illustrated in Fig. 9 for two different W/L_p ratios. The influence of the mooring stiffness seems similar for the two wave lengths considered in the figure. At the reflector tips, K_d reaches values above 1 due to wave diffraction. The same behaviour was obtained from the numerical simulations by Beels et al. (2010a).

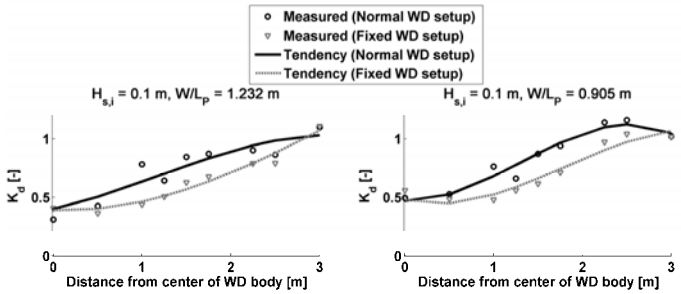

Fig. 9. Wave disturbance measured along a line behind the WD.

The average difference in K_d is determined by using Eq. 6 for the different considered W/L_p ratios and presented in Table 2. As seen, the difference in wave disturbance behind the WD is relatively unchanged for the different wave ratios.

$$K_{\mathrm{d,diff.}} = \frac{\sum K_{\mathrm{d,normal}} - \sum K_{\mathrm{d,fixed.}}}{\sum K_{\mathrm{d,fixed}}} \cdot 100\% \qquad (6)$$

Table 2. Difference between *"normal"* and *"fixed"* WD setup in wave disturbance behind the WD obtained from physical model tests.

W/L_p [-]	0.905	0.978	1.232
$K_{d,diff.}$ [%]	20.1	18.4	20.4

A small amount of scatter is obtained in the data for the *"normal"* setup in Fig. 9. This is mainly due to secondary wave radiation generated from the movements of the floating device. This "secondary" wave generation is illustrated further in Fig. 10, where the wave spectrum behind the WD body (measured from gauge C in Fig. 8) is

plotted for the *"normal"* and the *"fixed"* WD setup. As seen, an extra amount of energy is obtained at high frequencies for the *"normal"* WD setup.

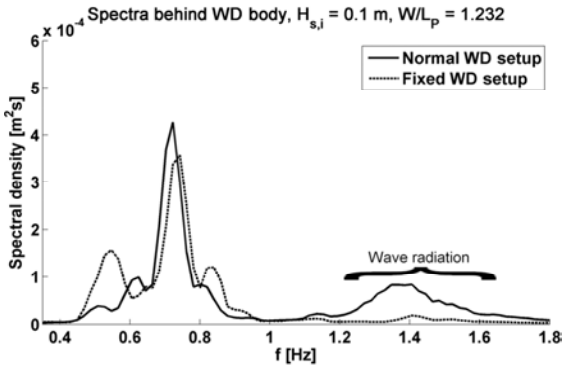

Fig. 10. Wave scatter generated by the floating WD.

IMPLEMENTATION IN WAVE PROPAGATION MODEL

Test data from the laboratory experiments is used to perform a calibration of the depth integrated MIKE21BW model by DHI. Due to the high influence from the mooring stiffness and wave lengths on the wave height reduction behind the WD, as concluded by Nørgaard et al (2011), different wave lengths and different mooring stiffness are implemented in MIKE21BW based on the physical model test results.

MIKE21BW is capable of reproducing combined effects of all important wave propagation phenomena such as diffraction, refraction, shoaling, wave breaking, non-linear wave-wave interaction, and bottom dissipation. Further, it can handle partial reflection and wave transmission from porous structures. The governing Boussinesq equations include nonlinearity as well as frequency dispersion.

MIKE21BW is a 2D depth integrated wave propagation model, and is thus not capable of accurately describing the wave propagation in the near-field of a floating structure due to the floating behaviour of the device. However, the equations in MIKE21BW have been modified to include porosity, and the effects of non-Darcy flow through a porous media. In this way, it is possible for MIKE21BW to simulate frequency dependent partial wave reflection, absorption and transmission.

Initially, the empty basin is implemented in the model by using sponge layers at fully absorbing boundaries, and porosity layers at partial reflecting boundaries. The empty basin is calibrated against reflection tests performed on the different boundaries, and against wave disturbances measured at different positions in the basin.

Secondly, the WD is implemented in the model using porosity layers which are tuned to obtain the measured wave disturbance behind the device. The calibration is performed by following the same approach as described in Beels et al. (2010b) where varying sponge layers are used to obtain the desired transmission characteristics for the different wave lengths considered. The geometry of the WD in the model is identical to the geometry of the model used in the laboratory, with slightly thicker reflectors however, due to the spatial grid discretization. The porosity layers of the basin boundaries and WD model, using the *"normal"* mooring setup, are illustrated in Fig. 11.

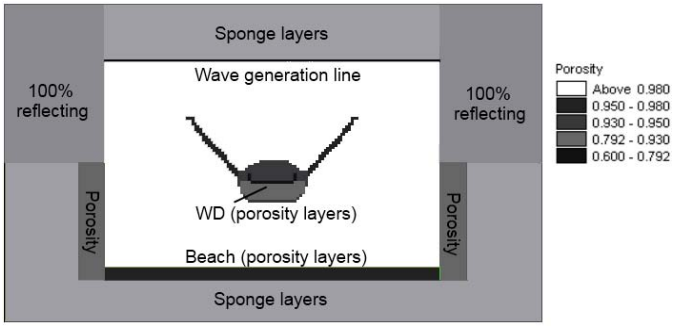

Fig. 11. Illustration of porosity layers used in model boundaries and WD geometry.

The dimensions of both the WD and the laboratory basin are converted from model scale, 1:51.8, to prototype scale, 1:1, for later implementation of the calibrated WD porosity layers in a 1:1 bathymetry. The spatial and temporal discretization used in the model is $dx = dy = 5.18$ *m* and $dt = 0.15$ *s*, respectively.

The WD in MIKE21BW is calibrated for wave length $W/L_p = 1.232$ and validated against $W/L_p = 0.905$. Since the MIKE21BW model is depth integrated, the model will very likely require another calibration for wave lengths outside this range. The calibration and validation is performed on both the *"normal"* setup and the *"fixed"* setup as illustrated in Fig. 12 and Fig. 13, respectively. A regression analysis is performed between the modelled and measured wave disturbances. Moreover, the percentage deviation between the measured and modelled transmitted wave power along the WD is determined by using Eq. 7. Results are shown in the figures. The calibration of the porosity layers was stopped when a difference of $P_{t,diff} \leq |5\%|$ was obtained.

$$P_{\text{t,diff.}} = \frac{\sum P_{\text{t,sim.}} - \sum P_{\text{t,meas.}}}{\sum P_{\text{t,meas.}}} \cdot 100\% \qquad (7)$$

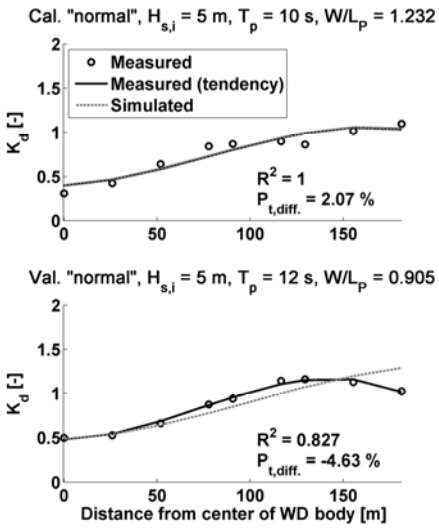

Fig. 12. Implementation of *"normal"* WD setup in MIKE21BW.

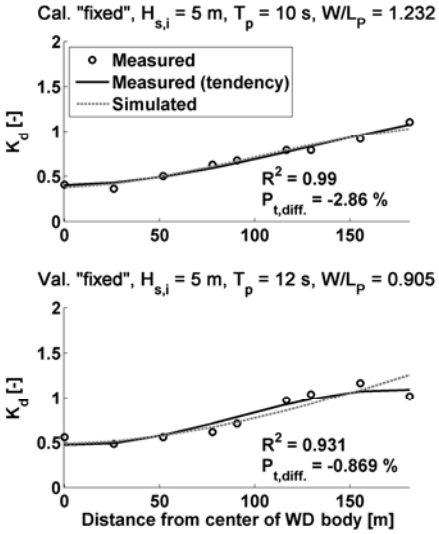

Fig. 13. Implementation of *"fixed"* WD setup in MIKE21BW.

As seen, a relatively good agreement is obtained between the modelled and measured K_d behind the WD. In the validation of the biggest considered wave lengths, it is difficult to obtain the correct wave disturbance at the reflector tips due to a relocation of the wave diffraction. However, due to the high values of K_d at this position (i.e. small wave height reduction), this deviation is accepted.

OVERALL NUMERICAL ESTIMATION OF WAVE TRANSMISSION FROM A SINGLE WD

The calibrated and validated porosity layers of the *"normal"* and *"fixed"* WD are implemented in a 3200 *x* 6000 *m* bathymetry with a uniform depth of *h* = 25 *m* (same depth as evaluated in the calibration/validation). A narrowed output area behind the device, with dimensions 2400 *x* 4000 *m*, is used to avoid wave disturbance from model boundaries such as diffraction from the sponge layers. The discretization is identical to the discretization used in the calibration/validation model. Surface elevation profile time series are obtained behind the WD with a length of 4000 *m* (across the output area). The bathymetry with the specified output area and the location of the WD are illustrated in Fig. 14.

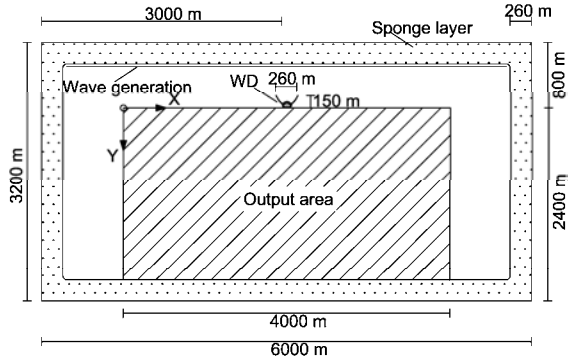

Fig. 14. Dimensions of bathymetry used to evaluate the wave transmission from the WD.

The simulated K_d across the output area at different distances behind the WD are illustrated in Fig. 15 for both the *"normal"* and *"fixed"* WD setups. K_d is again above one in the areas close to the reflector tips due to diffraction. In the study by Beels et al. (2010a), the areas with $K_d > 1$ was seen to fade out when evaluating short-crested waves. As expected, the wake widens at a distance farther behind the WD and becomes less significant as only a single device is considered and not a row of multiple devices.

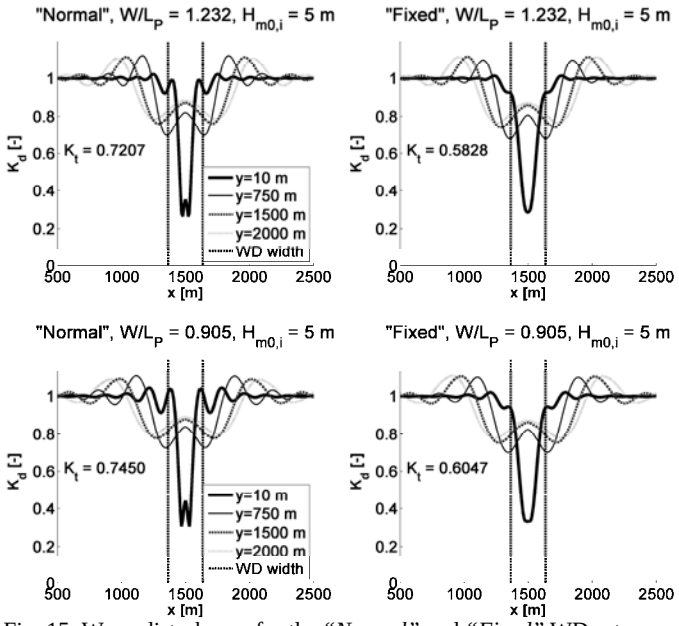

Fig. 15. Wave disturbance for the *"Normal"* and *"Fixed"* WD setup.

The overall wave transmission coefficient, K_t, is evaluated from a profile time series located in a distance of 10 *m* behind the WD. The transmitted wave power, p_t [*W/m*], and, P_t [*W*], is obtained from Eq. 8 where $C_g(f)$ is the group velocity and $S_t(f)$ is the transmitted wave energy spectrum. The incident wave power, p_i, and, P_i, is determined in the empty model without the presence of the WD.

$$C_g(f) = \frac{1}{2}\left(\frac{g}{k}\cdot\tanh(k(f)\cdot h)\right)^{1/2}\left(1+\frac{2\cdot k(f)\cdot h}{\sinh(2\cdot k(f)\cdot h)}\right)$$

$$p_t = \rho\cdot g\int_0^\infty C_g(f)\cdot S_t(f)df \qquad (8)$$

$$P_t = \rho\cdot g\int p_t dx$$

The power reduction behind the WD is distributed equally over the width of the device to obtain the overall transmission coefficient. The actual value of the wave absorption and wave reflection of the WD is unknown; however, the sum is given by:

$$p_{a,r} = p_a + p_r = \frac{P_i - P_t}{B} \qquad (9)$$

Finally, the overall wave transmission coefficient from the WD over a width of 260 *m* is determined using Eq. 10.

$$K_t = \sqrt{1-\frac{p_{a,r}}{p_i}} = \sqrt{1-\frac{(P_i - P_t)/B}{p_i}} \qquad (10)$$

K_t is plotted in Fig. 16 as a function of W/L_p for the *"normal"* and the *"fixed"* WD setup and compared to $K_{t,tot}$ from Fig. 6. Based on the fitted functions in Fig. 16, the wave transmission coefficients are seen to vary linearly within the relatively narrow considered range from

W/L_p = 0.905 to W/L_p = 1.232. The difference between the estimated wave transmission from the simple approach and the wave transmission from the calibrated model is further presented in the figure.

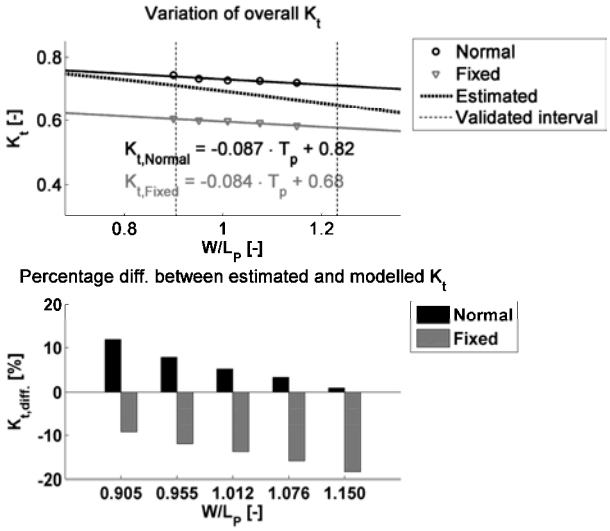

Fig. 16. Comparison of the overall K_t obtained from the calibrated model and K_t obtained by integration of wave power.

Within the validated range of wave periods, it can be concluded that the wave transmission coefficients obtained by wave power integration from the seabed to the draft of the WD provide results which are relatively close to the measured wave transmission from the calibrated model. The maximum deviation is found to be 18 % for the fixed mooring. The wave transmission coefficients obtained from integration of wave power and from the *"fixed"* WD setup was expected to be almost identical. However, this does not seem to be the case. Especially for the highest evaluated wave lengths in Fig. 16 where the wave transmission coefficients from integration seem to be more similar to the wave transmission obtained from the *"normal"* WD setup. This discrepancy is caused by the simplifications made in the approach of integration of energy from the draft of the WD to the seabed using Eq. 1. The integration is based on linear wave theory, and it is assumed that all wave power from the draft to the seabed is fully transmitted which is not correct due to viscosity effects etc. below the draft of the floating structure and at the seabed. The neglected viscosity in the integration of wave energy will result in an overestimated wave transmission as observed in Fig. 16. The simplified model is, however, still seen to provide a rough estimate of the wave transmission coefficient.

An almost constant difference in the wave transmission coefficients for the *"normal"* and *"fixed"* setups of approximately 23 % is obtained when evaluating the different wave periods (or wave lengths). A constant difference was also obtained from the wave disturbance coefficients measured behind the WD as presented in Table 2.

WAVE TRANSMISSION FROM MULTIPLE WDs

In the study of Beels et al. (2010a), it was found that five WDs installed in a staggered grid with an individual distance of 2·B would produce 5 times the electricity as from a single WD in a North Sea wave climate, as the available incident wave power for the second row was not affected by the first row. Therefore, tt is interesting to determine whether the wave transmission from a farm of 5 WDs is similar to the wave transmission from single WD.

The WD farm in Fig. 17 is considered - with a total width of 1300 *m*. The individual WDs are positioned with a distance of 260 *m* and 340 *m* between the reflector tips which, according to Beels et al. (2010a), is sufficient in order to avoid collisions. In this case, an individual distance of B is used in the two rows to avoid unprotected areas in the wake behind the devices.

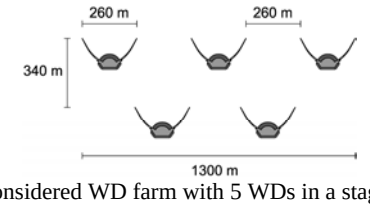

Fig. 17. Considered WD farm with 5 WDs in a staggered grid.

The wave transmission behind the WD farm is determined using the same approach as for the single WD. The *"Normal"* WD setup is considered. Results are illustrated in Fig. 18 and compared to the wave transmission from a single WD.

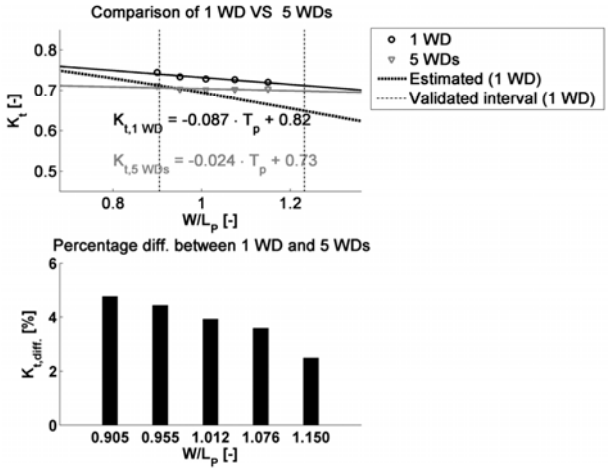

Fig. 18. Comparison of K_t from a single and multiple WDs.

As seen in Fig. 18, the wave transmission behind 5 staggered WDs is slightly reduced compared to a single WD. However, a maximum difference of approximately 5% is obtained within the considered interval of W/L_p, and thus K_t from a single WD and 5 staggered WDs can be concluded to be relatively similar. Furthermore, when using a distance of B in the farm (which is more suitable for coastal protection), the wave power is only slightly reduced in front of the WDs in the second row.

SIMPLE IMPLEMENTATION OF WD MODEL

Instead of implementing the WD in MIKE21BW using the exact geometry, it is interesting to determine whether a simplified geometry, such as a rectangular box with implementation of the overall transmission coefficient, is sufficient in order to evaluate the wave height reduction behind the device. The simplified structure is implemented in the model at the centreline of the correct geometry.

The wave height reduction from the exact and simplified geometries at a distance of y = 10 *m* and y = 2000 *m* respectively is illustrated in Fig. 19. As seen, a significant difference in K_d is present in a short distance behind the WD (y = 10 *m*). However, the variation in K_d along the output line at a distance farther behind the WD (y = 2000 *m*), becomes quite similar to the correct and calibrated model.

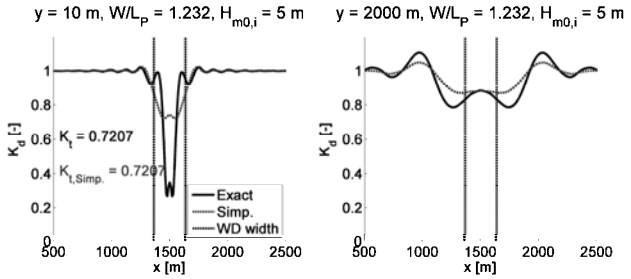

Fig. 19. Wave disturbance at different distances behind the WD using homogeneous porosity layers for the "*Normal* WD setup.

The simplified geometry of the WD is positioned in a staggered grid of 5 WDs, corresponding to the layout in Fig. 17. The porosity layers of the simplified WDs are calibrated to have the same K_t as the exact geometry of a single "*normal"* WD. In Fig. 20 K_d behind the exact and simplified geometries is compared. K_d becomes very similar at a distance farther behind the WDs.

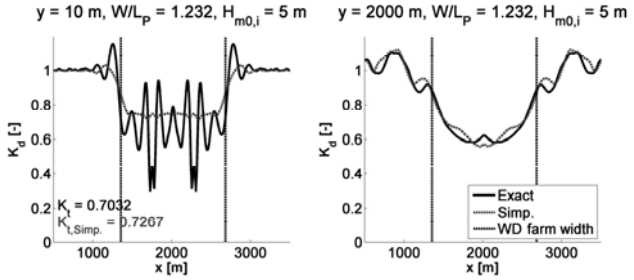

Fig. 20. Illustration of conversion from the exact WD geometry into a homogeneous rectangle of porosity layers.

CONCLUSIONS

The floating Wave Dragon wave energy converter has been implemented in the depth integrated MIKE21BW Boussinesq model. The model was calibrated and validated against previous published physical model test results on the wave height reduction measured behind the device. Different stiffness in the mooring system has been considered. The calibration and validation has indicated that the porosity layers in the depth integrated MIKE21BW model were well suited for modelling the wave disturbance behind a floating structure. A maximum deviation of 4.63 % was obtained between the measured and simulated transmitted wave power behind the device.

Based on simulations in the calibrated model, approximately 23 % higher wave transmission with the normal mooring stiffness was obtained compared to a fixed device in various considered sea states. Thus, the transmission of wave power through the floating device was found to be relatively sensitive to the stiffness in the mooring system. The simplified approach for obtaining the wave transmission coefficient behind the WD, based on wave power integration below the draft of the device, provided results which were in the range between the wave transmission coefficient obtained from MIKE21BW, using the normal mooring setup, and a fixed device. The maximum deviation between estimated and modelled transmission was approximately 18 %.

The simplified approach can thus be used as a rough estimate on the wave transmission from the Wave Dragon, and is believed to be suitable for estimating the wave transmission through other types of floating devices such as floating breakwaters.

When evaluating a farm of 5 WDs positioned in a staggered grid with an individual distance of B, the total K_t from the farm was similar to the wave transmission from a single WD. Results have further shown the possibility of implementing both a single and multiple WDs in MIKE21BW using simplified geometry with a constant K_t. This leads is to the possibility of performing a simpler implementation of floating wave energy devices in wave propagation models.

The present study has been focusing solely on long-crested waves. On-going study is focusing on the influence from short-crested waves on the wave transmission behind the devices.

ACKNOWLEDGEMENTS

The support of the European Commission through FP7.2009-1, Contract 244104 - THESEUS ("*Innovative technologies for safer European coasts in a changing climate*"), is gratefully acknowledged.

REFERENCES

Beels, C., Troch, P., Visch, K.D., Kofoed, J.P. and Backer, G.D. (2010a), *"Application of the Time-Dependent Mild-Slope Equations for the Simulation of Wake Effects in the Lee of a Farm of Wave Dragon Wave Energy Converters"*, Renewable Energy, vol 35, nr. 8.

Beels C., Troch P., De Backer G., Vantorre M., and De Rouck J. (2010b). *"Numerical implementation and sensitivity analysis of a wave energy converter in a time-dependent mild-slope equation model"*. Coastal Engineering, Volume 57, Issue 5, May 2010

Frigaard, P., Tedd, J., Kofoed, J. P., and Friis-Madsen, E. (2006). *"3 Years Experience with Energy Production on the Nissum Bredning Wave Dragon Prototype"*. In Proceedings of the Fourth CA-OE Workshop, Lisbon, 16-17 November, 2006

Hald, T. and Frigaard, P.: (2001), *"Forces and Overtopping on 2. Generation Wave Dragon for Nissum Bredning, Phase 3 project, Danish Energy Agency."* Project no: ENS-51191/00 - 0067. AAU

Kofoed, J.P. and Burcharth, H.F. (2002), *"Estimation of Overtopping Rates on Slopes in Wave Power Devices and Other Low Crested Structures"*, Proceedings of the 28th International Conference on Coastal Engineering : ICCE '02: Cardiff, Wales, UK

Kramer, M.M. and Frigaard, P.B. (2002), *"Efficient Wave Energy Amplification with Wave Reflectors"*, Proceedings of the Twelfth (2002) International Offshore and Polar Engineering Conference, Kitakyushu, Japan, ISOPE, s. 707-712.

Nørgaard, JH, Andersen, TL and Kofoed, JP (2011), *"Wave Dragon Wave Energy Converters Used as Coastal Protection: a physical model test study"*, Coastal Structures 2011: International Conference September 6-8, 2011 Yokohama, Japan

Palha, A. Mendes L., Fortes C.J, Melo A.B, and Sarmento A. (2010). *"The impact of wave energy farms in the shoreline wave climate: Portuguese pilot zone case study using Pelamis energy wave devices."* Renewable Energy, 35(1), p.62-77.

Ruol, P., Zanuttigh, B., Martinelli, L., Kofoed, J. P., and Frigaard, P. (2011). *"Near-Shore Floating Wave Energy Converters: applications for coastal protection."* I Smith, J. M., & Lynett, P. (red.), Coastal Engineering 2010: Proceedings of the 32nd International Conference on Coastal Engineering.

Venugopal, V. and Smith, G., (2007). *"Wave climate investigation for an array of wave power devices."* In Proceedings of the 7th European Wave and Tidal Energy Conference. IST/IDMEC.

Zanuttigh, B., Martinelli, L., Castagnetti, M., Ruol, P., Kofoed, J. P., & Frigaard, P. (2010). *"Integration of Wave Energy Converters into Coastal Protection Schemes."* In Proceedings of the 3rd International Conference and Exhibition on Ocean Energy: ICOE 2010